**RESEARCH ARTICLE**

# Quasi-Gradient Nonlinear Simplex Optimization Method in Electromagnetics

**ARMAN AFSARI** [1], (Member, IEEE), **AMIN ABBOSH** [2], (Fellow, IEEE), **AND YAHYA RAHMAT-SAMII** [3], (Life Fellow, IEEE)

[1]Electrical Engineering Department, University of Wisconsin–Madison, Madison, WI 53706, USA
[2]School of Information Technology and Electrical Engineering, The University of Queensland, Brisbane, QLD 4072, Australia
[3]Electrical Engineering Department, University of California at Los Angeles, Los Angeles, CA 90095, USA

Corresponding author: Arman Afsari (aafsari@wisc.edu)

**ABSTRACT** Particle swarm optimization (PSO), genetic algorithm (GA), and nonlinear simplex optimization method (SOM) are some of the most prominent gradient-free optimization algorithms in engineering. When it comes to a common group of electromagnetic optimization problems wherein less than 10 optimization parameters are present in the problem domain, SOM features faster convergence rate vs PSO and GA. Nevertheless, PSO and GA still outperform SOM by having more accuracy in finding the global minimum. To improve the accuracy of SOM in problems with few optimization parameters, a quasi-gradient (Q-G) search direction is added to the conventional algorithm. An extra decision is made by the proposed algorithm to move alongside the reflection or quasi-gradient direction during the error-reduction operations. This modification will improve the accuracy of SOM, which otherwise fails in the examples presented in this article, to levels similar to PSO and GA, while retaining approximately 33% faster convergence speed with relatively small number of parameters, and 20% faster convergence speed with larger number of optimization parameters. Following a standard benchmark test verification, the proposed algorithm successfully solves a suite of electromagnetic optimization problems. Representative examples include the optimization of absorber dimensions in an anechoic chamber, and estimation of the properties of an unknown embedded object by scattered microwave signals.

**INDEX TERMS** Device optimization, gradient-free optimization, heuristic methods, parameter estimation, quasi-gradient optimization.

## I. INTRODUCTION

Gradient-free optimization is key to modern engineering [1]. In a diverse range of electromagnetic applications ranging from enhancing the urban wireless coverage [2], to improving the radiation characteristics of antennas as single elements [3], or designing the antenna arrays [4], performing adaptive beamforming by antenna arrays [5], and improving the directivity of antenna arrays [6], there are some parameters that must be optimized to retain the desired performance. Moreover, parameter estimation in electromagnetic inverse problems is another venue where the gradient-free optimization can demonstrate unique features [7], [8]. Such a solid demand has led to significant progress in heuristic

and metaheuristic gradient-free optimization methods in electromagnetics like particle swarm optimization (PSO) [9], genetic algorithm (GA) [10], and nonlinear simplex optimization method (SOM) [11].

### A. GRADIENT-FREE OPTIMIZATION: SPEED AND ACCURACY

The computational time of most of the gradient-free optimization methods increases exponentially by the number of optimization parameters [12]. Regarding the simplicity of programming the algorithm of SOM as a local-search method, and the smaller number of candidate points during optimization, the method shows faster convergence speed vs PSO and GA as long as the number of optimization parameters is relatively low (say below 10) and the

optimization problem is rather simple in terms of noise and number of local minima [1]. For instance, in [1, Table 1] and [1, Table 4 ], the success rate of SOM is only 3% when dealing with objective functions like Quadruple with 20 optimization parameters, but its convergence speed is 27 times faster than GA. However, the population-based nature of PSO [13] and GA [14] as global-search methods can handle up to hundreds of parameters. From this perspective, PSO and GA may be privileged with respect to SOM [1].

Considering the accuracy of solution, the gradient-free methods have a heuristic nature and directly evaluate the objective function in each iterative run [15]. If the distribution of the population (candidate points) in each iterative run inherits some randomness, which is the case in the metaheuristic methods like PSO and GA [9], [10], the solution of the gradient-free method is subject to unrepeatability [16]. In other words, for the same problem with the same conditions, two different runs of the same metaheuristic gradient-free algorithm will return two slightly different solutions. Though these solutions are usually accurate, there are some optimization problems with complicated or noisy objective functions where a typical run of the gradient-free method may fail to return an accurate solution. This issue is usually referred to as the success rate of the gradient-free methods [1]. SOM, on the other hand, has a deterministic distribution of candidate points and returns the same solution in different runs. Nonetheless, the local-search nature of SOM that involves few candidate points in each run may result in an occasionally lower accuracy with respect to PSO and GA as global-search methods [1].

### B. SOM: MOTIVATION AND POTENTIAL
Yet, many practical electromagnetic optimization problems like those in Fig. 1 have less than 10 optimization parameters. Since the convergence speed of SOM in problems with small number of optimization parameters is faster than PSO and GA, and the algorithm possesses a deterministic nature, improving the accuracy of the algorithm can make SOM as a very competitive and attractive gradient-free algorithm in electromagnetics. Moreover, the simplicity of programming the algorithm of SOM is another attractive feature to implement the method in electromagnetics. As such, the motivation of proposing the quasi-gradient SOM (Q-GSOM) in this article is to improve the accuracy of SOM for those electromagnetic optimization problems containing relatively low number of optimization parameters. In passing, we note that SOM is sometimes referred to as downhill or Nelder-Mead optimization method in the literature [17].

In the rest of this article, the main difference between the gradient-free and gradient-based optimization methods is discussed briefly in Section II. The difference in the differentiability of the objective function of the gradient-free and gradient-based methods is the main inspiring point to add an extra decision-making step to SOM in Section III. Per an approximate linear search direction of the gradient

of the objective function of SOM, the algorithm decides to whether or not move alongside the approximate direction of the gradient. This search decision reduces the chance of local minima failures. By running a benchmark test on Q-GSOM, PSO, and GA, it is observed in Section IV that the Q-GSOM can attain an accuracy similar to PSO and GA, while retaining a faster convergence speed. In Section V, Q-GSOM successfully solves the optimization problems in Fig. 1. Finally, conclusions are made in Section VI.

## II. GRADIENT-FREE VS GRADIENT-BASED OPTIMIZATION
Gradient-free methods directly evaluate the objective function to find its global extremum point, while the gradient-based methods search for the global extremum point alongside a direction in which the gradient (derivative) of the objective function with respect to the optimization parameters vanishes [18].

Fig. 1 shows the above difference between the gradient-free and gradient-based methods in practice. Gradient-free methods require an initial topology to define the parameters on which the optimization is performed. For instance, Fig. 1(a) shows a common shape optimization problem in electromagnetic interference and compatibility tests wherein the initial dimensions $(a, b, c)$ of the absorbers in an anechoic chamber are regarded as optimization parameters. As another example, Fig. 1(b) depicts a microwave monitoring problem. The initial topology of this inverse problem is seen in Fig. 1(c) where the changes of relative permittivity $\varepsilon_r$, conductivity $\sigma$, and diameter $d$ of the circular object embedded inside the cylindrical structure are monitored (details of the monitoring system are given in [19]). The final values of these parameters will be given, and graphically shown in Section V.

Gradient-based methods, however, reconstructs the entire topology. As such, they do not need any initial topology to start from. For instance, the microwave monitoring problem in Fig. 1(b) can be treated by gradient-based optimization as well (say Born iterative method [20], [21]) where the reconstructed topology of $\varepsilon_r$ and $\sigma$, (functions of space coordinates (x,y,z)), are seen in Figs. 1(d) and 1(e), respectively. Accordingly, the gradient-free and gradient-based optimization methods are sometimes referred to as the shape and topology optimizations, respectively [22].

### A. DEFINITION OF THE OBJECTIVE FUNCTION
To clarify the definition of the objective function (F) in the above examples, let us consider the corresponding pointwise objective functions in Fig. 1 as,

$$\text{Fig.1(a)} : F = \int_W \left| \vec{E}_{sct}(a, b, c, x, y, z) \right|^2$$

$$dW \rightarrow 0, \text{ on walls } (W)$$

$$\text{Fig.1(b)} : F = \left| \vec{E}_{sct}(\varepsilon_r, \sigma, d, x, y, z) - \vec{\alpha}S \right|^2$$

$$\rightarrow 0, \text{ on apertures} \tag{1a}$$
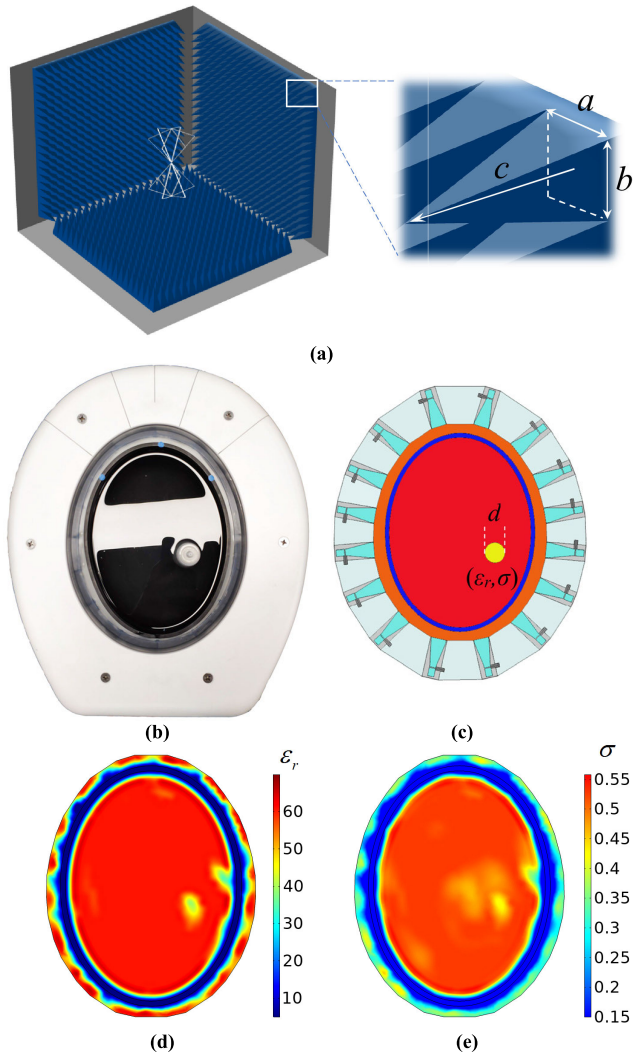
**FIGURE 1.** Examples of gradient-free optimization in real-world electromagnetics are seen in (a) and (b). Difference between the gradient-free and gradient-based optimization, when treating (b), is seen in (c) to (e), respectively. (a) Anechoic chamber optimized by gradient-free optimization, (b) Microwave monitoring, (c) Initial topology of (b), (d) Gradient-based optimization of $\varepsilon_r$, (e) Gradient-based optimization of $\sigma$.

where $\vec{E}_{sct}$, $\vec{\alpha}$, and $S$ are the scattered field, calibration vector, and measured S-parameters, respectively [23]. In either case, $\vec{E}_{sct}$ is defined by the vector wave equation as,

$$\vec{E}_{sct} = \left( \frac{1}{\omega_0^2 \mu_0 \varepsilon_0 \varepsilon_r} \vec{\nabla} \times \left( \vec{\nabla} \times \vec{E} \right) - \chi \vec{E} - \vec{E}_{inc} \right) + \frac{j}{\omega_0 \varepsilon_0 \varepsilon_r} \sigma \vec{E} \qquad (1b)$$

and is summed over the walls of the anechoic chamber in Fig. 1(a) and over the apertures in Fig. 1(b). Quantities $\omega_0$, $\mu_0$, $\varepsilon_0$, and $\chi = \varepsilon / \varepsilon_b - 1$ are respectively the free-space angular frequency, permeability, permittivity, and electric susceptibility defined by complex permittivity $\varepsilon = \varepsilon_r + \sigma / j\omega$ [24], [25]. Moreover, the total electric field is the summation of the incident and scattered fields as $\vec{E} = \vec{E}_{inc} + \vec{E}_{sct}$. In addition,

$\vec{\nabla}$ is the gradient operator, and $j = \sqrt{-1}$ is the unit of imaginary numbers.

### B. PROPOSAL: Q-GSOM
SOM possesses five successive error-reduction operations called reflection, expansion, forward contraction, backward contraction, and shrink, graphically shown in Fig. 2 [1]. The reflection operation is key to the next four operations as it determines the search direction on which the other four operations are established. Inspired by the gradient-based methods, we add an extra evaluation step to the reflection operation. The algorithm then decides on two possible search directions: The conventional direction that evaluates the objective function, and a new direction that evaluates the gradient of the linearly-approximated objective function in the space of parameters (say quasi-gradient direction) [26]. Such a quasi-gradient search direction will improve the accuracy of SOM by reducing the chance of being trapped in local minima, while retaining the efficiency of SOM [1].

## III. Q-GSOM ALGORITHM
In this section, Q-GSOM is proposed. The approach aims at achieving similar accuracy as GA and PSO in problems with relatively small number of optimization parameters, while retaining higher computational speed.

### A. INITIALIZATION
Let us assume that there are $N$ parameters needed to be optimized as $(x_1, x_2, \ldots, x_N)$. The initial values of these parameters can be expressed by a vector like $\mathbf{X_0} = (x_{10}, x_{20}, \ldots, x_{N0})$. Clearly, $\mathbf{X_0}$ is taken from an initial topology as Fig. 1(a) or 1(c). In addition to $\mathbf{X_0}$, the variation range of these parameters are defined to form the solution space $(x_{\min}, x_{\max}$ of each parameter). This space is demonstrated in Fig. 2(a) for $N = 3$ (selected for ease of graphical demonstration of different steps).

To optimize $(x_1, x_2, \ldots, x_N)$, we first construct an equilateral "simplex" (generalized triangle) with $N + 1$ vertices within the space of parameters shown in Fig. 2(a). One of the vertices is the initial guess $\mathbf{X_0}$. All other vertices with equal distance $c_0$ are derived by adding the following vectors to this initial guess as,

$$\mathbf{X_1} = \mathbf{X_0} + (p, q, q, \ldots, q)$$
$$\mathbf{X_2} = \mathbf{X_0} + (q, p, q, \ldots, q)$$
$$\vdots$$
$$\mathbf{X_N} = \mathbf{X_0} + (q, q, q, \ldots, p) \qquad (2)$$

where $q = \frac{c_0}{N\sqrt{2}}(\sqrt{N+1} - 1)$ and $p = q + \frac{c_0}{\sqrt{2}}$.

Typically, $c_0 = 1$ to allow the algorithm to search in a sufficiently large volume at early iterations. Moreover, as measurement noise (appeared in the S-parameter in Fig. 1(b)) may result in the same frequency response for two very close vertices, locating the vertices far enough (distanced with $c \geq 1$) makes the algorithm robust with respect to noise. The immediate contrast between SOM and GA or PSO is
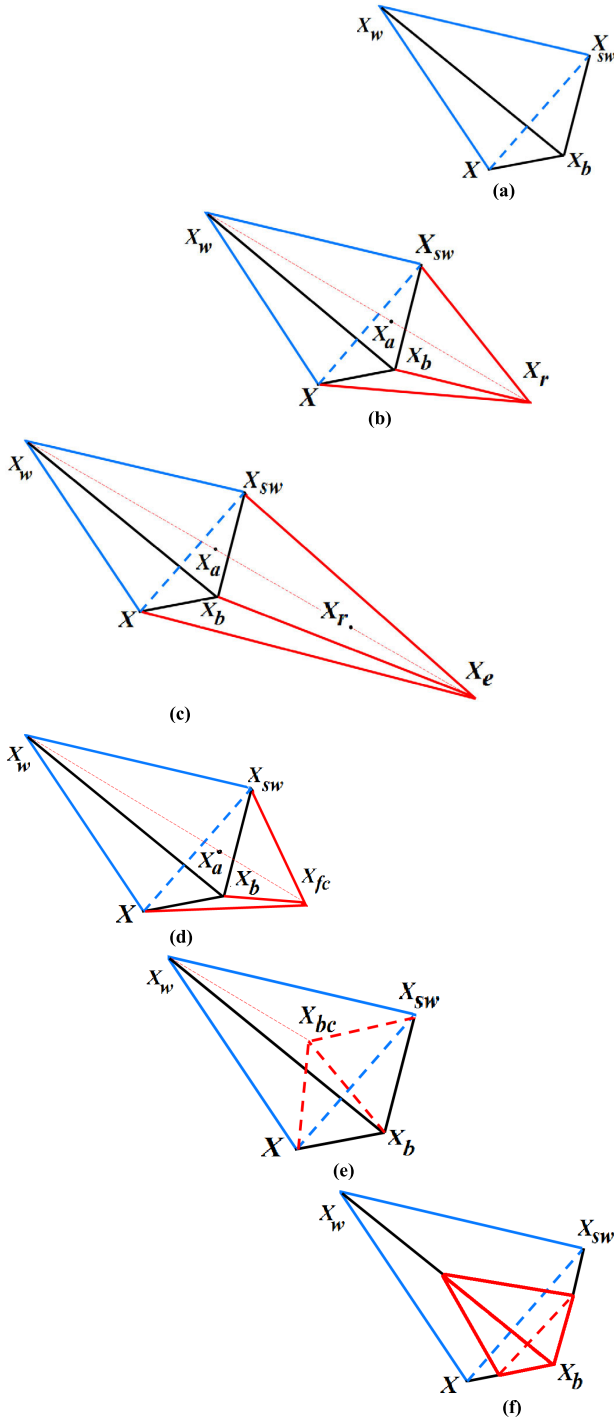
**FIGURE 2.** Different error-reduction operations of SOM are graphically demonstrated for $N = 3$. In all the operations, $\mathbf{X}_w$ is replaced by a new vertex. In shrinking, all the vertices except $\mathbf{X}_b$ are replaced by new vertices. (a) Simplex, (b) Reflection, (c) Expansion, (d) Forward contraction, (e) Backward contraction, (f) Shrinking.

recognized by (2). First, the population of SOM is fixed at $N + 1$ vertices (candidate points), while PSO and GA have much larger populations that can be adjusted almost freely. Second, constructing a simplex forms a local search domain, while PSO and GA distribute their populations across the

entire space of parameters to form a global search method. Third, the initial distribution of candidate points in PSO and GA is generally random, while SOM distributes its candidate points in a deterministic manner [9], [10] (unless $c_0$ is chosen randomly).

By constructing the simplex, the next step is to evaluate the objective function $F(x_1, x_2, \ldots, x_N)$ at every vertex $\mathbf{X}_0, \mathbf{X}_1, \ldots, \mathbf{X}_N$. After evaluating the objective function in all the vertices, three vertices possess special importance for SOM. The vertex which gives the least value of F is called the "best" vertex and is denoted as $\mathbf{X}_b$. On the contrary, the vertex with the highest mismatch is called the "worst" vertex $\mathbf{X}_w$. To guide the algorithm into a direction that always reduces the highest mismatch, we also need an auxiliary point wherein F has the second highest value (mismatch). This vertex is called the "second worst" vertex or $\mathbf{X}_{sw}$. After this arrangement, the average value of all the vertices except $\mathbf{X}_w$ is calculated and called $\mathbf{X}_a$. The reason for excluding $\mathbf{X}_w$ from averaging is to maintain the line segment between $\mathbf{X}_a$ and $\mathbf{X}_w$ ($L_{\mathbf{X}_w\mathbf{X}_a}$) always downward. This is because $L_{\mathbf{X}_w\mathbf{X}_a}$ contains some useful points in which F may have lower mismatch than $\mathbf{X}_w$ during the optimization process. In Fig. 2(a), we take $\mathbf{X}$ as a representative for all the other vertices.

### B. ERROR-REDUCTION OPERATIONS

After the above initialization, the method performs at least two, and utmost five "error-reduction" operations to minimize F. In each of these steps, the old value of $\mathbf{X}_w$ is removed from the computer memory (not restored for the next iteration), and all the other vertices are rearranged to have new $\mathbf{X}_b$, $\mathbf{X}_w$, and $\mathbf{X}_{sw}$. Hereafter, these operations are discussed.

### 1) REFLECTION

The first optimization step in Q-GSOM is to reflect the worst vertex $\mathbf{X}_w$. There are two directions of reflection that we wish to consider here. First, reflection across $L_{\mathbf{X}_w\mathbf{X}_a}$ with the same length as,

$$\mathbf{X}_r = 2\mathbf{X}_a - \mathbf{X}_w \qquad (3)$$

shown in Fig. 2(b) is considered. This operation is to check if moving in the $L_{\mathbf{X}_w\mathbf{X}_a}$ direction should be continued by the algorithm or another direction will lead the algorithm to the optimum vertex. Second, reflection across the quasi-gradient (Q-G) direction of the following hyperplane is considered. This hyperplane is regarded as the linear approximation of F within the space of parameters,

$$F = [a_0, a_1, \ldots, a_N] [1, x_1, \ldots, x_N]^T \qquad (4a)$$

At each vertex we have,

$$F(\mathbf{X}_0) = [a_0, a_1, \ldots, a_N] [1, x_{10}, \ldots, x_{N0}]^T$$
$$F(\mathbf{X}_1) = [a_0, a_1, \ldots, a_N] [1, x_{11}, \ldots, x_{N1}]^T$$
$$\vdots$$
$$F(\mathbf{X}_N) = [a_0, a_1, \ldots, a_N] [1, x_{1N}, \ldots, x_{NN}]^T \qquad (4b)$$
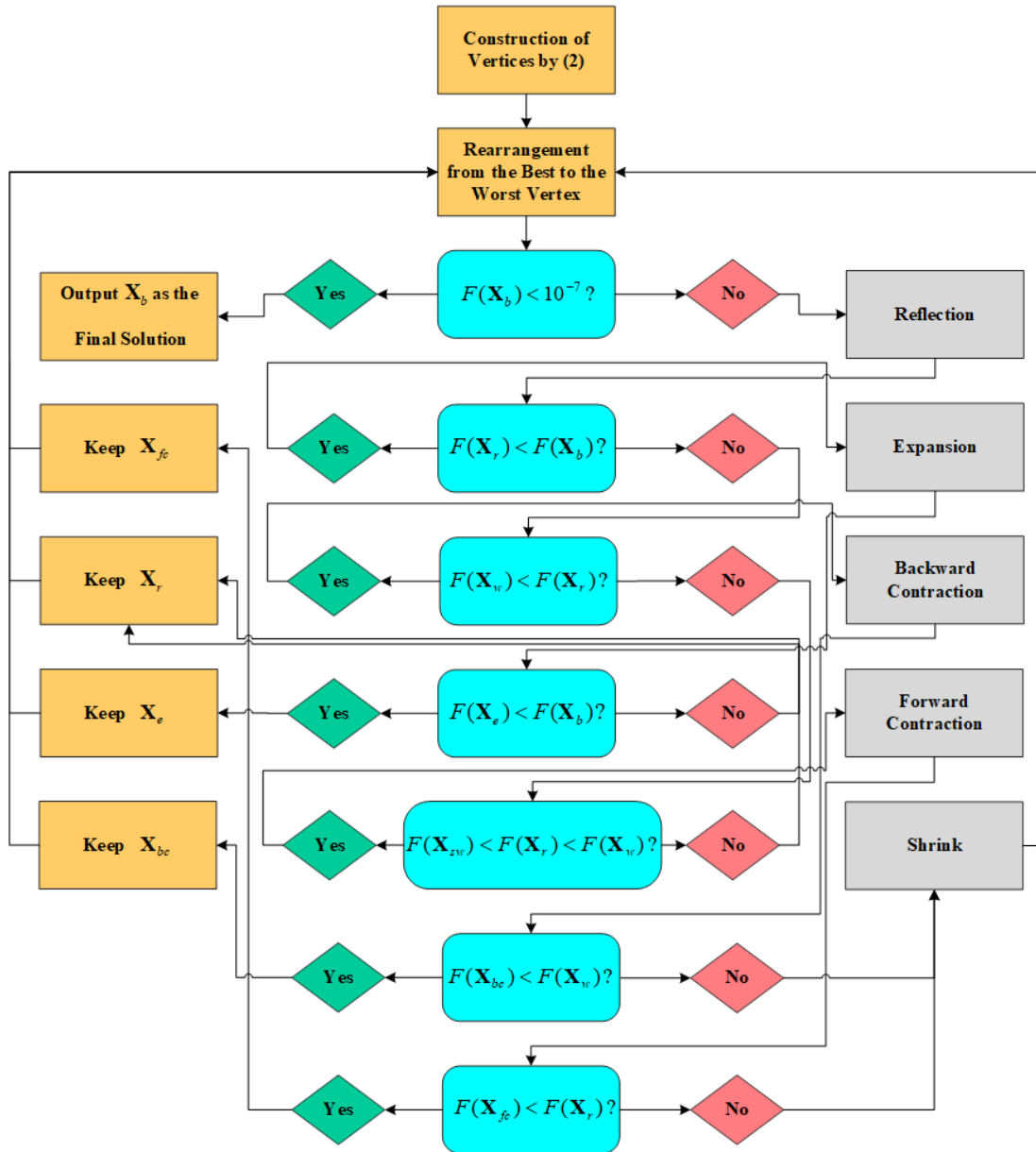
**FIGURE 3.** Flowchart of Q-GSOM algorithm.

where "$T$" is the transpose operator and $(x_{10}, \ldots, x_{N0})$ is the vector of parameter values constructing the initial point $\mathbf{X}_0$ (and so on). The coefficient matrix is thus derived as,

$$[a_0, a_1, \ldots, a_N]$$

$$= \begin{bmatrix} F(\mathbf{X}_0) \\ F(\mathbf{X}_1) \\ \vdots \\ F(\mathbf{X}_N) \end{bmatrix}^T \left( \begin{bmatrix} 1 & x_{10} & \cdots & x_{N0} \\ 1 & x_{11} & \cdots & x_{N1} \\ \vdots & \vdots & \ddots & \vdots \\ 1 & x_{1N} & \cdots & x_{NN} \end{bmatrix}^T \right)^{-1} \quad (4c)$$

As such, the second reflection direction is chosen alongside the quasi-gradient vector as,

$$\mathbf{X}_r = \mathbf{X}_a + \frac{1}{||[a_0, a_1, \ldots, a_N]||} [a_0, a_1, \ldots, a_N] \quad (5)$$

This quasi-gradient direction reduces the chance of search in a direction ending at a local minimum. Q-GSOM evaluates F at two reflected points in (3) and (5), and selects the reflection point with lower F. If F has a lower mismatch at the selected $\mathbf{X}_r$ with respect to $\mathbf{X}_b$, that is $F(\mathbf{X}_r) < F(\mathbf{X}_b)$, before replacing the following,

$$\mathbf{X}_w \leftarrow \mathbf{X}_r \quad (6)$$

(we use the programming convention $A \leftarrow B$ to show that the old value of $A$ is substituted by the new value of $B$), the algorithm evaluates the possibility of finding even a better vertex. To this end, the expansion operation is performed by further moving in the same direction of the selected $\mathbf{X}_r$.

| Algorithm 1 Q-GSOM Execution Steps | |
|---|---|
| **Steps** | **Commands** |
| | **Input:** parameters $(x_1, x_2, \ldots, x_N)$ |
| | **Input** : variation range $x_{\min}$ and $x_{\max}$ |
| 1: | **Input: $\mathbf{X}_0$** |
| | **Input: F** |
| | **Do:** vertex construction: eq. (2) |
| 2: | **Do:** vertex rearrangement: Fig. 2(a) |
| | **Do:** calculation of $\mathbf{X}_a$ |
| | **if** (12) is satisfied |
| |   **Output: $\mathbf{X}_b$** |
| | **else** |
| |   **Do** : Reflection |
| |   **if** $F(\mathbf{X}_r) < F(\mathbf{X}_b)$ |
| |     **Do** : Expansion |
| |     **if** $F(\mathbf{X}_e) < F(\mathbf{X}_b)$ |
| |       **Do:** (8) |
| |       **Return:** Step 2 |
| |     **else** |
| |       **Do:** (6) |
| |       **Return:** Step 2 |
| |     **end** |
| |   **else if** $F(\mathbf{X}_w) < F(\mathbf{X}_r)$ |
| |     **Do:** Backward Contraction |
| |     **if** $F(\mathbf{X}_{bc}) < F(\mathbf{X}_w)$ |
| |       **Do: $\mathbf{X}_w \leftarrow \mathbf{X}_{bc}$** |
| |       **Return:** Step 2 |
| 3: |     **else** |
| |       **Do:** Shrink |
| |       **Return:** Step 2 |
| |     **end** |
| |   **else if** $F(\mathbf{X}_{sw}) < F(\mathbf{X}_r) < F(\mathbf{X}_w)$ |
| |     **Do:** Forward Contraction |
| |     **if** $F(\mathbf{X}_{fc}) < F(\mathbf{X}_r)$ |
| |       **Do:$\mathbf{X}_w \leftarrow \mathbf{X}_{fc}$** |
| |       **Return:Step 2** |
| |     **else** |
| |       **Do:Shrink** |
| |       **Return:Step 2** |
| |     **end** |
| |   **else** |
| |     **Do: $\mathbf{X}_w \leftarrow \mathbf{X}_r$** |
| |     **Return:Step 2** |
| |   **end** |
| |   **end** |
| |   **end** |
| | **end** |

## 2) EXPANSION

As per Fig. 2(c), the algorithm further moves alongside $L_{\mathbf{X}_w \mathbf{X}_a}$ or the quasi-gradient vector with the same step-length i.e.,

$$\mathbf{X}_e = 2\mathbf{X}_r - \mathbf{X}_a \qquad (7)$$

Then, F is also evaluated at this expansion vertex. If its value is lower than $F(\mathbf{X}_b)$ i.e., $F(\mathbf{X}_e) < F(\mathbf{X}_b)$ (even if $F(\mathbf{X}_e) > F(\mathbf{X}_r)$), the algorithm replaces the following,

$$\mathbf{X}_w \leftarrow \mathbf{X}_e \qquad (8)$$

and (iteratively) returns to the reflection step after rearranging the new vertices from the worst to the best. The reason that the algorithm does not immediately accept $\mathbf{X}_w \leftarrow \mathbf{X}_r$, while it is the best-found vertex among the other vertices, comes from the fact that this vertex is reserved by the algorithm as it lies inside the new simplex formed by $\mathbf{X}_e$. Hence, by performing the expansion, we merely safeguard the neighborhood domain of $\mathbf{X}_r$ wherein some other good or even better vertices may exist to minimize F. If $F(\mathbf{X}_e)$ is not lower than $F(\mathbf{X}_b)$, we perform (6) and iteratively return to the first operation i.e., reflection, after rearranging the new vertices from the worst to the best. Hence, the minimum number of error-reduction operations is two.

### 3) FORWARD CONTRACTION

Either (6) or (8) assumes $F(\mathbf{X}_r) < F(\mathbf{X}_b)$. If this is not the case, but $F(\mathbf{X}_{sw}) < F(\mathbf{X}_r) < F(\mathbf{X}_w)$, we conclude that the algorithm has excessively moved along $L_{\mathbf{X}_w \mathbf{X}_a}$ or the quasi-gradient direction, and better vertices may lie at distances closer than $\mathbf{X}_r$. We thus perform the forward contraction by returning half a step-length (typically the balanced step-length) from $\mathbf{X}_r$ toward $\mathbf{X}_a$ as seen in Fig. 2(d), i.e.,

$$\mathbf{X}_{fc} = 1.5\mathbf{X}_a - 0.5\mathbf{X}_w$$
$$or$$
$$\mathbf{X}_{fc} = \mathbf{X}_a + 0.5 \frac{1}{|[a_0, a_1, \ldots, a_N]|} [a_0, a_1, \ldots, a_N] \qquad (9)$$

depending on the chosen direction of search. If $F(\mathbf{X}_{fc}) < F(\mathbf{X}_r)$, we form a new simplex on vertices $\mathbf{X}, \mathbf{X}_b, \mathbf{X}_{sw}, \mathbf{X}_{fc}$ by returning to the initialization step and rearranging these new vertices from the "worst" to the "best" one.

### 4) BACKWARD CONTRACTION

If $F(\mathbf{X}_w) < F(\mathbf{X}_r)$, to still hope that $L_{\mathbf{X}_w \mathbf{X}_a}$ or the quasi-gradient direction contains some vertices that can improve the mismatch in F, in the same way as forward contraction we perform the backward contraction by moving backward half a step-size from $\mathbf{X}_a$ toward $\mathbf{X}_w$, as shown in Fig. 2(e),

$$\mathbf{X}_{bc} = 0.5\mathbf{X}_a + 0.5\mathbf{X}_w$$
$$\mathbf{X}_{fc} = \mathbf{X}_a - 0.5 \frac{1}{|[a_0, a_1, \ldots, a_N]|} [a_0, a_1, \ldots, a_N] \qquad (10)$$

If $F(\mathbf{X}_{bc}) < F(\mathbf{X}_w)$, a new simplex seen in Fig. 2(e) is constructed on $\mathbf{X}, \mathbf{X}_b, \mathbf{X}_{sw}, \mathbf{X}_{bc}$ by returning to the initialization step and rearranging the vertices from the worst to the best.

### 5) SHRINKING

If, however, none of the above situations takes place, the last step to find the better direction toward the optimum vertex

**TABLE 1.** Benchmark test.

| Runs \ N | Q-GSOM Griewank 3 | 9 | Q-GSOM Rastrigin 3 | 9 | Q-GSOM Rosenbrock 3 | 9 | PSO Griewank 3 | 9 | PSO Rastrigin 3 | 9 | PSO Rosenbrock 3 | 9 | GA Griewank 3 | 9 | GA Rastrigin 3 | 9 | GA Rosenbrock 3 | 9 |
|---|---|---|---|---|---|---|---|---|---|---|---|---|---|---|---|---|---|---|
| 1 | -6.1 | -1.2 | -18.3 | -2.1 | **11.2** | 24.7 | -6.2 | **-5.5** | -18.1 | **-2.3** | 12.2 | 26.3 | -6.1 | -1.1 | -17 | -1.7 | 11.3 | 25.1 |
| 2 | -6.1 | -1.2 | -18.3 | -2.1 | **11.2** | 24.7 | **-6.3** | -4.9 | -18.1 | -1.8 | 12.2 | 26.1 | -6.1 | -1.6 | -18 | -1.7 | **11.2** | 24.8 |
| 3 | -6.1 | -1.2 | -18.3 | -2.1 | **11.2** | 24.7 | -6.2 | -5.1 | -18.1 | -1.7 | 12.1 | 25.9 | **-6.3** | -0.9 | -18 | -1.8 | 11.3 | **23.2** |
| 4 | -6.1 | -1.2 | -18.3 | -2.1 | **11.2** | 24.7 | -6.2 | -5.0 | **-20.2** | -2.05 | 12.2 | 26.1 | -6.2 | -1.2 | -17 | -1.7 | 12.0 | 24.1 |
| 5 | -6.1 | -1.2 | -18.3 | -2.1 | **11.2** | 24.7 | -6.1 | -5.2 | -18.1 | -1.9 | 13.1 | 25.7 | -6.1 | -1.0 | -18 | -1.9 | 12.1 | 23.9 |
| 6 | -6.1 | -1.2 | -18.3 | -2.1 | **11.2** | 24.7 | -6.2 | -5.1 | -18.2 | -1.8 | 13.0 | 26.0 | **-6.3** | -1.2 | -18 | -1.7 | 12.1 | 24.3 |
| 7 | -6.1 | -1.2 | -18.3 | -2.1 | **11.2** | 24.7 | -6.2 | -5.1 | -19.6 | -1.9 | 12.5 | 26.1 | **-6.3** | -1.1 | -18 | -1.8 | 12.0 | 24.1 |
| 8 | -6.1 | -1.2 | -18.3 | -2.1 | **11.2** | 24.7 | -6.2 | -5.3 | -17.9 | -2.1 | 12.1 | 26.1 | -6.1 | -1.3 | -20 | -1.8 | **11.2** | 24.1 |
| 9 | -6.1 | -1.2 | -18.3 | -2.1 | **11.2** | 24.7 | -6.2 | -5.2 | -18.1 | -2.1 | 12.1 | 25.9 | **-6.3** | -1.1 | -18 | -1.9 | 12.0 | 24.2 |
| 10 | -6.1 | -1.2 | -18.3 | -2.1 | **11.2** | 24.7 | -6.2 | -5.2 | -18.1 | -2.1 | 12.1 | 26.1 | -6.1 | -1.0 | -18 | -1.1 | 12.0 | 24.1 |
| Time (s) | **0.42** | **7.31** | **0.44** | **7.91** | **0.43** | **7.58** | 0.63 | 8.1 | 0.68 | 8.7 | 0.66 | 8.3 | 0.67 | 9.06 | 0.71 | 9.21 | 0.7 | 9.14 |

| Runs \ N | SOM Griewank 3 | 9 | SOM Rastrigin 3 | 9 | SOM Rosenbrock 3 | 9 |
|---|---|---|---|---|---|---|
| 1 | -1.8 | 6.3 | -7.5 | 4.9 | 17.8 | 31.3 |
| 2 | -1.8 | 6.3 | -7.5 | 4.9 | 17.8 | 31.3 |
| 3 | -1.8 | 6.3 | -7.5 | 4.9 | 17.8 | 31.3 |
| 4 | -1.8 | 6.3 | -7.5 | 4.9 | 17.8 | 31.3 |
| 5 | -1.8 | 6.3 | -7.5 | 4.9 | 17.8 | 31.3 |
| 6 | -1.8 | 6.3 | -7.5 | 4.9 | 17.8 | 31.3 |
| 7 | -1.8 | 6.3 | -7.5 | 4.9 | 17.8 | 31.3 |
| 8 | -1.8 | 6.3 | -7.5 | 4.9 | 17.8 | 31.3 |
| 9 | -1.8 | 6.3 | -7.5 | 4.9 | 17.8 | 31.3 |
| 10 | -1.8 | 6.3 | -7.5 | 4.9 | 17.8 | 31.3 |
| Time (s) | 0.38 | 6.46 | 0.39 | 7.01 | 0.37 | 6.21 |

Total number of iterations is set to 3000 for all the methods. A 64-bit computer platform with Intel(R) Xeon(R) E-2186M CPU and 128 GB RAM is used to run the algorithms. Function values are in dB. Bold tables show a superior performance across a specific benchmark test. GA and PSO evaluations are approximately 35791 and 33000.

is to shrink the simplex. To this end, we only keep the best vertex $\mathbf{X}_b$, and for the other vertices, say $i$th one, the shrinking operation is performed as

$$\mathbf{X}_i(new) = 0.5\mathbf{X}_b + 0.5\mathbf{X}_i(old) \qquad (11)$$

Then, the proposed algorithm returns to initialization step to rearrange the new vertices formed in the shrinking step shown in Fig. 2(f). The whole iterative process is continued, until F($\mathbf{X}_b$) meets the truncation condition of the objective function, say reaching a small number $\delta$,

$$\mathrm{F}(\mathbf{X}_b) \leq \delta \qquad (12)$$

The value of $\mathbf{X}_b$ that satisfies the truncation condition is stored as the final solution. To demonstrate all these steps at once, Fig. 3 shows the corresponding flowchart of the Q-GSOM to better show the order of operations. In addition, Algorithm 1 shows the programming steps of Q-GSOM in MATLAB. In the next section, three common benchmark tests are performed on Q-GSOM, GA, and PSO to evaluate their relative accuracy and speed. We implement MATLAB functions GA and PSO for this comparison with the default setting.

## IV. BENCHMARK TEST
Different mathematical functions have been introduced as merits to evaluate the performance of gradient-free optimization methods. Amongst, Griewank, Rastrigin, and Rosenbrock functions are the most common benchmarks to assess the capability of gradient-free optimization methods in electromagnetics [9]; mainly, because these functions can resemble some of the most common objective functions in electromagnetics. In addition, they have their global minimum at zero.

In this section, the performance of Q-GSOM in dealing with these three functions is evaluated with respect to SOM, PSO and GA in MATLAB. In all the comparisons, we run the algorithms 10 times to consider the success rate of PSO and GA. Moreover, the number of optimization parameters $N$ is once set to 3 and once to 9 in Table 1. This is to compare the relative convergence speed of the above algorithms, first for a very small $N$ to demonstrate the superiority of Q-GSOM, and then for a larger value of $N$ above which the Q-GSOM is incapable of showing any superiority. As discussed, Q-GSOM is of particular interest in problems with low number of optimization parameters. It is observed that in all the benchmark test, SOM error level can be considered

as failure when compared to the other three methods. Similar test failures were observed in [1].

## A. GRIEWANK FUNCTION

Griewank function can evaluate the performance of a gradient-free optimization method in dealing with strong but low-frequency noise present in the problem domain. On a large scale seen in Fig. 4a, the function looks like a smooth function that has been contaminated by strong unwanted noise. When zoomed into the global minimum in Fig. 4(b), the sinusoidal noise is better observed across the solution space. The function is defined as,

$$F_{Gr} = \frac{1}{4000} \sum_{i=1}^{N} x_i^2 - \prod_{i=1}^{N} \cos(\frac{x_i}{\sqrt{i}}) + 1 \qquad (13)$$

Table 1 demonstrates the performance of Q-GSOM with respect to PSO and GA in minimizing the Griewank function. While both PSO and GA can attain the lowest minimum value (in dB) during the benchmark test, Q-GSOM reaches almost the same accuracy as PSO and GA with roughly 33% lower computational time when $N = 3$. Even for large $N$, Q-GSOM can compete with GA in accuracy, while retaining a faster convergence speed.

## B. RASTRIGIN FUNCTION

Rastrigin function is a complementary assessment tool to the previous step, when weak but high-frequency noise is present in the problem domain. On a large scale, the function looks very smooth in Fig. 4(c). When zoomed in, however, many local minima and maxima are observed across the solution space in Fig. 4(d). This test is of particular importance when estimating the properties of some inaccessible parameters by some weak and noisy scattered microwave signals recorded at some observation points like Fig. 1(b). The wave-like variation of this smooth function provides a proper benchmark assessment for objective functions defined per the high-frequency electromagnetic fields. The function is defined as,

$$F_{Ra} = \sum_{i=1}^{N} \left( x_i^2 - 10 \cos(2\pi x_i) + 10 \right) \qquad (14)$$

In Table 1, Q-GSOM demonstrates approximately 34% lower computational time to minimize the above function for small $N$ when compared to PSO and GA. Though PSO can achieve the best accuracy for small and large $N$, Q-GSOM shows a marginally better accuracy with respect to GA for large $N$.

## C. ROSENBROCK FUNCTION

Rosenbrock function is a complementary assessment tool to the previous two steps, when the objective function has a stationary nature across the space of parameters as seen in Fig. 4(e). In electromagnetics, this is the case when objective functions are defined per the static fields, or per the stationary quantities of electromagnetic fields like energy. It is a challenging function to minimize, as the descent direction from

any point to the global minimum has a very low steepness, with numerous "good" solutions as shown in Fig. 4(f). Later on, it will be seen that this assessment is directly relevant to Fig. 1(a) where the initial values of *a,b,c* are "good" enough. The function is defined as,

$$F_{Ro} = \sum_{i=1}^{N-1} \left( 100(x_{i+1} - x_i^2)^2 + (x_i - 1)^2 \right) \qquad (15)$$

The quasi-gradient essence of Q-GSOM described by (5) is best implemented in this test where PSO and GA might not be able to compete. Table 1 shows that for small $N$, Q-GSOM can perform better than PSO in both the accuracy and computational time. In comparison with GA, Q-GSOM possesses significant 38% faster speed. For large $N$, GA performs slightly better in accuracy when compared to Q-GSOM, but the computational time of GA is still 17% higher than Q-GSOM.

By concluding this section, it is worth mentioning that per many experiments, larger $N$ ($>10$) would gradually result in an inefficient computational time and improper accuracy for Q-GSOM with respect to PSO and GA. The reason mainly comes from the global-search nature of PSO and GA that randomly scatter their populations across the entire problem domain. This makes them more robust in optimization problems with very large $N$ [9], [10]. Hence, we limit Q-GSOM to those electromagnetic optimization problems that possess a relatively small $N$. Overall, Q-GSOM can attain approximately 33% faster speed when $N$ is small, and approximately 20% faster convergence speed when $N$ is around 9.

## V. Q-GSOM IN ELECTROMAGNETICS

The performance of the Q-GSOM is attractive in many electromagnetic problems having a few optimization parameters, as those discussed in Fig. 1. In this section, Q-GSOM, PSO, GA, and SOM are implemented in optimizing two general types of problems in electromagnetics. First, the methods are implemented to optimize the dimensions of the absorbers in Fig. 1(a) to reduce the scattered fields from the walls of an anechoic chamber. Second, an inverse problem in electromagnetics is studied in Fig. 1(b) to monitor the change of properties of an embedded object. The demonstrated figures in this section are in dB scale, as the corresponding electromagnetic quantities are either small in value (like scattered field) or traditionally better understood in dB scale (like resistive loss). We implemented COMSOL Multiphysics Livelink with MATLAB to run the optimization algorithms. The objective functions of these examples were already given in (1a). It will be seen that SOM cannot compete with the other 3 methods. Moreover, it will be seen that Q-GSOM possesses faster speed with respect to GA and PSO, while their error degrees are comparable. As such, graphical results of Q-GSOM are only shown, as the method outstands in both accuracy and speed.
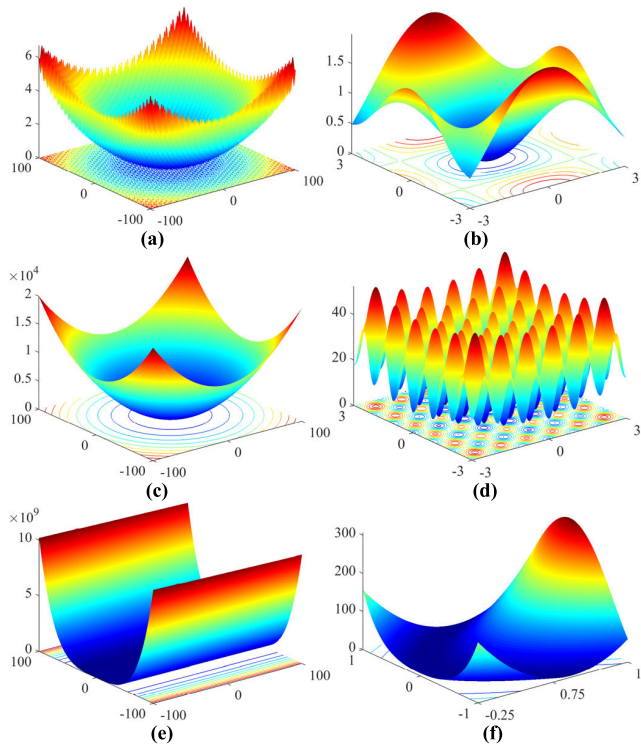
**FIGURE 4.** Griewank, Rastrigin, and Rosenbrock test functions in (a), (c), and (e), with their zoomed figures around their global minimum in (b), (d), and (f), respectively.

## A. OPTIMIZING THE ABSORBERS OF ANECHOIC CHAMBER

The proper performance of absorbers within an anechoic chamber is critical to accurately evaluate the characteristics of antennas in infinite domain, or assess the interference and compatibility of electromagnetic devices [27]. The pyramidal arrays of absorbers in Fig. 1(a) are designated to guide the electromagnetic field towards their adjacent absorbers and then dissipate the field via their conductive material. By absorbing these fields and shielding the chamber versus unwanted signals coming from outside, the chamber acts theoretically as an infinite domain.

The cubic chamber with 8 m$^3$ volume in Fig. 1(a) is supported by arrays of absorbers with initial dimensions as $a = 15$, $b = 15$, $c = 40$ in cm. We assume that the dielectric properties of the absorber are fixed at $\sigma = 0.5$, $\varepsilon_r = 1$. A bi-conical antenna common in assessing the interference and compatibility is placed at the center of chamber, operating at 240 MHz. The goal is to check if the initial dimensions set in COMSOL is optimum, or better dimensions exist for the absorber to improve the performance of the chamber. Introducing these three parameters within the Q-GSOM, the optimized problem is seen in Fig. 5. In Figs. 5(a) and 5(b), a comparison between the initial and final norms of the electric field show slight improvement in the performance of the chamber in eliminating the scattered fields. Weaker field strength reaches the chamber walls in Fig. 5(b). Figs. 5(c) and 5(d) show the same fields inside the chamber before and after

optimization. While the fields possess almost the same pattern, contours of the fields after optimization show certain uniformity across the absorbers in comparison with the initial fields. This uniformity is a demonstration of higher agreement between the optimized absorbers and their theoretical counterpart i.e., the scattering boundary condition used to truncate the domain computationally [26]. The absorption and conversion of fields to heat is shown in Figs. 5(e) and 5(f), before and after optimization. As seen, the generated heat follows a better horizontal pattern in Fig. 5(f) when compared to Fig. 5(e). This is due to a slight change in the dimensions of the optimized absorber with respect to its initial dimensions. The change applied by Q-GSOM is based on the radiation pattern of the bi-conical antenna, which shows its maximum intensity across the azimuth (xy) plane. Q-GSOM takes advantage of this radiation pattern by slightly increasing the parameter $a = 15.23$ and decreasing the parameter $b = 14.76$ during optimization shown in Fig. 5(g). To more effectively absorb the fields, the sharpness of the pyramid slightly increases to $c = 40.41$. Error degree of Q-QSOM is comparable with GA in Fig. 5(h), while the Q-GSOM is faster by almost 30% as discussed hereafter.

In running the algorithm, we let the iterations continue by 10 units once the objective function no longer changes remarkably. This is to ensure that Q-GSOM no longer replaces the converged point. The space of parameters is constructed by extending the variation range of each parameter by 40% above and below its initial value. The initial dimensions of parameters in this example were intentionally chosen to give a very good initial solution. The purpose was to assess if Q-GSOM fed by a very good initial value will fall into the initial local minima or can escape it and converge to a better solution. Moreover, we tried to avoid initial dimensions that are not realistic. In Subsection V-B, however, the assessment situation will be relatively opposite.

The total computational time for optimizing the problem is 41.34 minutes. Per the Rosenbrock benchmark test, marginally better dimensions of absorber might still be achievable by multiple runs of GA. Table 2 summarizes the computational times of different methods.

## B. PARAMETER ESTIMATION IN MICROWAVE MONITORING

In microwave monitoring, the change of properties of inaccessible objects are studied over time [28]. The remarkable penetration of electromagnetic fields provide possibility to monitor the objects not directly accessible for measurements. Examples include through-wall imaging to find cracks and leakage in concrete or pipes [29], or medical monitoring to evaluate the treatment progress [30], [31].

Fig. 1(b) shows a microwave monitoring setup wherein the monitoring antennas successively illuminate the domain in a clockwise pattern. An object with initial properties as $d = 15$, $\sigma = 0.4$, $\varepsilon_r = 30$ is embedded inside an elliptic plastic container having the approximate semi-minor and semi-major axes 7 cm and 10 cm, respectively, and 0.5 cm

**(a)** **(b)**

**(c)** **(d)**

**(e)** **(f)**

**(g)**

**(h)**
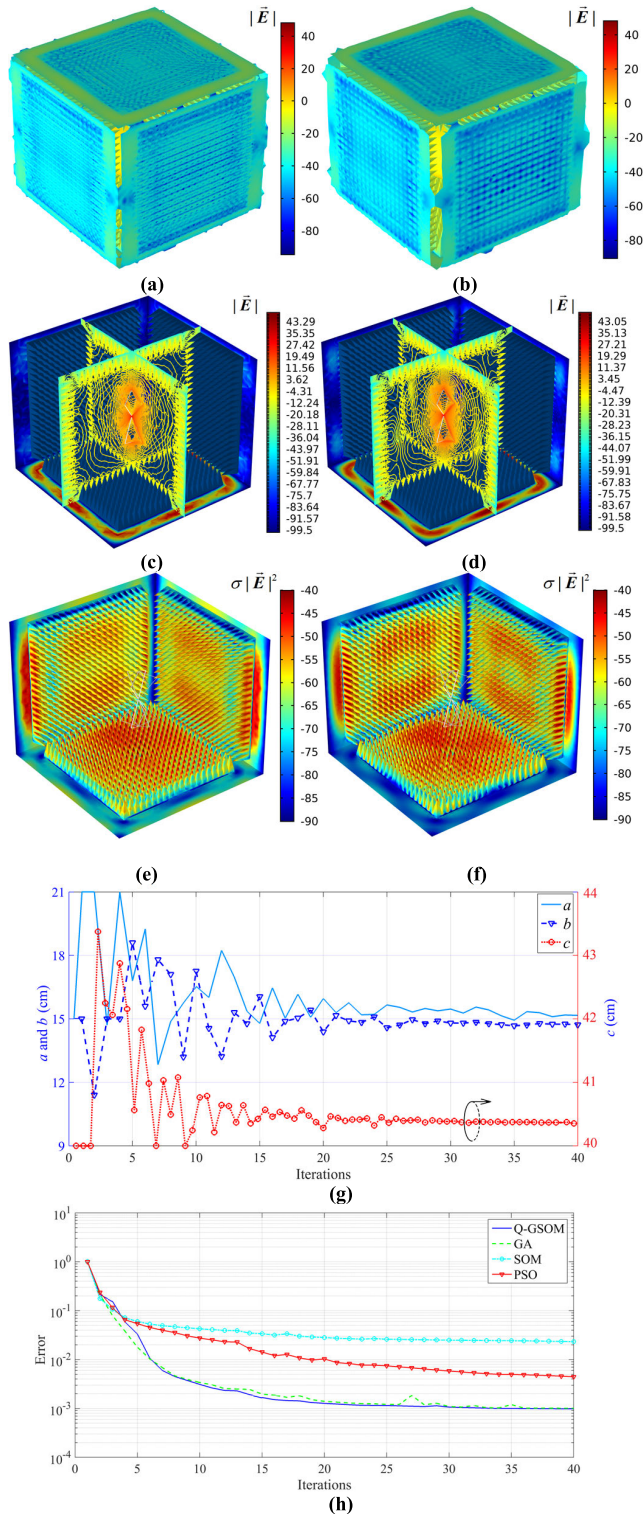
**FIGURE 5.** Optimized absorber in an anechoic chamber. (a) Initial electric field norm on the walls (Volt/m). (b) Final electric field norm on the walls (Volt/m). (c) Contour of the initial electric field norm inside the chamber (Volt/m). (d) Contour of the final electric field norm inside the chamber (Volt/m). (e) Initial resistive loss over the absorbers (W/m3). (f) Final resistive loss over the absorbers (W/m3). (g) Values of optimization parameters versus iteration number. (h) Convergence error.

thickness. The container is filled with a liquid with fixed properties $\sigma = 0.5$, $\varepsilon_r = 60$ at 780 MHz. To provide a better



**(a)** **(b)**

**(c)** **(d)**

**(e)**

**(f)**
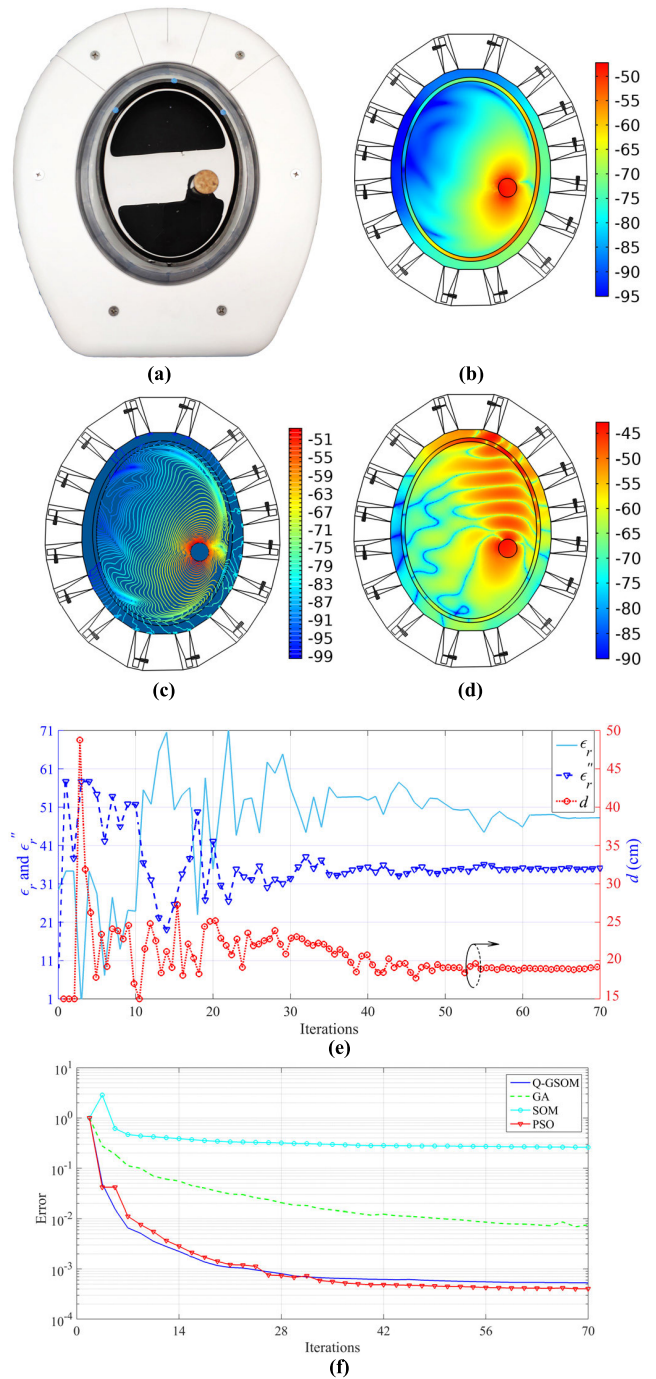
**FIGURE 6.** Parameter estimation of the circular object initiated in Fig. 1(b). (a) Replaced object with different diameter and dielectric properties. (b) Scattered electric field by the estimated object when antenna number 1 is in transmit mode. (c) Contour of the scattered electric field by the estimated object when antenna number 1 is in transmit mode. (d) Resistive loss caused by the estimated object when antenna number 1 is in transmit mode. (e) Estimated parameters per iteration. (f) Convergence error.

matching between the antennas and the domain, a coupling liquid with the fixed properties $\sigma = 0.2$, $\varepsilon_r = 52$ entirely fills the gap between the antenna apertures and the plastic container. The 16 horn-like waveguide antennas have an aperture size of $1.5 \times 3.5$ cm$^2$, and are loaded by ceramic with

approximate fixed properties $\sigma = 0.01, \varepsilon_r = 45$. The cross section of the entire system is shown in Fig. 1(c).

The goal is to estimate accurately the change in the properties of the embedded cylindrical object. To this end, the object is replaced by another object with different properties as $d = 20, \sigma = 1.5, \varepsilon_r = 47$ shown in Fig. 6(a). The objects are replaced by hand to consider the effect of imperfect positioning when estimating the properties of the new object.

Taking Fig. 1(c) as the initial setup, the scattered fields at the beginning of the optimization process are apparently zero. The final estimated object by Q-GSOM contributes in scattering the electric fields (dB) as shown in Fig. 6(b) when antenna number 1 is in transmit mode. This antenna is chosen generically as the estimated object repeats similar scattering behavior with respect to all the other antennas in transmit mode. The contours of the scattered fields in Fig. 6(c) show how all the other antennas sense the estimated object when antenna number 1 is in transmit mode. As the object is highly conductive, the resistive loss generated by the estimated object across the domain is considerably high in Fig. 6(d) when antenna number 1 is in transmit mode. The final estimated.

The space of parameters are chosen relatively large with respect to initial value i.e. $0 < d < 50$ and $1 < \varepsilon_r, \varepsilon_r'' < 71$. To provide consistency in the variation ranges of Fig. 6(e), $\varepsilon_r'' = \sigma/\omega\varepsilon_0$ represents $\sigma$. The computational time taken to estimate the properties of the new object across the cross-section in Fig. 1(c) is 4.68 minutes with reasonable estimation accuracy with respect to the other prominent methods i.e., PSO and GA in Table 2. Per the Rastrigin benchmark test, negligibly better estimations might be achievable by PSO at the expense of multiple runs. Regarding the positioning errors, unavoidable noise in $S$, and slight nonlinear scattering effects that does not exactly hold the calibration relation $\vec{E}_{sct} = \vec{\alpha}S$ [32], longer iterations are needed by Q-GSOM to stabilize the variations of the objective function and parameters. Error plots in Fig. 6(f) depict the similarity of PSO and Q-GSOM in accuracy, while Q-GSOM is 18% faster.

Before concluding the discussions, we recall that the benchmark assessment was performed against GA and PSO, because these methods are well-established and widely used. Nonetheless, there are plenty of other gradient-free methods in electromagnetics possessing their own features when compared to GA and PSO. Some of the examples include other swarm intelligence methods discussed in [33], or different optimization approaches in neural network [34] and machine learning [17].

**TABLE 2.** Convergence speed in electromagnetic problems.

| Problem | Q-GSOM | PSO | GA | SOM |
|---------|--------|------|-------|-------|
| Fig. 5 | 41.34 | 55.71 | 59.18 | 36.73 |
| Fig. 6 | 4.68 | 5.71 | 6.13 | 3.54 |

Computational times are in minutes.

In addition, it is worth noticing that the applications discussed in this article are merely some representative examples of electromagnetic optimization problems with a few number of optimization parameters. The proposed method can be applied to many relevant problems like semiconductor device optimization [35], phased-array 5G mm-wave smartphone optimization [36], MIMO antenna optimization [37], and full-duplex antenna inter-port optimization [38].

### C. COMPARISON WITH OTHER SOM-BASED METHODS
Finally, there are other prominent works on SOM that improved the accuracy of the original version of SOM. In addition to [1] that was tailored for electromagnetic problems in this paper, an interesting weighting method has been proposed in [39] to reposition the average point $\mathbf{X}_a$ to the center of the simplex side formed by $\mathbf{X}, \mathbf{X}_b, \mathbf{X}_{sw}$ in Fig. 2. There are, however, two fundamental differences between Q-GSOM and the weighting method in [39]. First, the method in [39] totally replaces the average point $\mathbf{X}_a$ by the weighted point, and takes the reflection step as,

$$\mathbf{X}_r = \frac{1}{|[a_0, a_1, \dots, a_N]|} [a_0, a_1, \dots, a_N] \quad (16)$$

This type of reflection becomes extremely biased to one or some of the vertices with large values. Though the chance of approaching the global minimum increases, the chance of being trapped by local minima increases at the same time, if the biasing vertices lead the search direction towards the local minima. Including the average point during reflection operation will include the effect of all the vertices and reduces the chance of being trapped by local minima. In other words, vertices with extreme values are moderated during the search steps.

The second difference between the method presented in this paper and the method in [39] is the way that the weighting (coefficient) matrix is calculated. In [39], the weighting matrix is calculated for each vertex with respect to $\mathbf{X}_w$ as, (17) shown at the bottom of the page.

As such, no hyperplane is formed on all the vertices to evaluate the approximate direction of gradient. The gradients in [39] are isolated from each other, evaluated individually

$$[a_0, a_1, \dots, a_{N-1}] = \begin{bmatrix} |\mathrm{F}(\mathbf{X}_0) - \mathrm{F}(\mathbf{X}_w)| \\ |\mathrm{F}(\mathbf{X}_1) - \mathrm{F}(\mathbf{X}_w)| \\ \vdots \\ |\mathrm{F}(\mathbf{X}_{N-1}) - \mathrm{F}(\mathbf{X}_w)| \end{bmatrix}^T \left( \begin{bmatrix} 1 & |x_{10} - x_{1w}| & \cdots & |x_{N0} - x_{Nw}| \\ 1 & |x_{11} - x_{1w}| & \cdots & |x_{N1} - x_{Nw}| \\ \vdots & \vdots & \ddots & \vdots \\ 1 & |x_{1(N-1)} - x_{1w}| & \cdots & |x_{(N-1)(N-1)} - x_{(N-1)w}| \end{bmatrix}^T \right)^{-1} \quad (17)$$

**IEEE** *Access*

A. Afsari et al.: Quasi-Gradient Nonlinear Simplex Optimization Method in Electromagnetics

versus $\mathbf{X}_w$. As such, if one vertex shows significant gradient, the algorithm will move into the direction of the gradient of that vertex, regardless of ensuring if that direction leads to the global minimum or not.

## VI. CONCLUSION

The added quasi-gradient feature to SOM can assist the algorithm to more effectively search for the global minimum in an electromagnetic optimization problem. The quasi-gradient feature provides wider search directions for the algorithm when finding the global minimum. The extra decision-making step on choosing the search direction in each iteration levels up the algorithm to compete with some of the prominent gradient-free optimization methods like PSO and GA during standard benchmark tests. When implemented in electromagnetics, the proposed method named Q-GSOM demonstrates reliable performance in both parameter optimization and parameter estimation, as long as the number of optimization parameters is relatively low. Representative examples included an anechoic chamber optimization and a microwave monitoring measurement.

## REFERENCES

[1] N. Pham, A. Malinowski, and T. Bartczak, "Comparative study of derivative free optimization algorithms," *IEEE Trans. Ind. Informat.*, vol. 7, no. 4, pp. 592–600, Nov. 2011.

[2] P. Rocca, P. D. Rù, N. Anselmi, M. Salucci, G. Oliveri, D. Erricolo, and A. Massa, "On the design of modular reflecting EM skins for enhanced urban wireless coverage," *IEEE Trans. Antennas Propag.*, vol. 70, no. 10, pp. 8771–8784, Oct. 2022, doi: 10.1109/TAP.2022.3146870.

[3] A. Pietrenko-Dabrowska and S. Koziel, "Generalized formulation of response features for reliable optimization of antenna input characteristics," *IEEE Trans. Antennas Propag.*, vol. 70, no. 5, pp. 3733–3748, May 2022, doi: 10.1109/TAP.2021.3137405.

[4] Q. Xu, S. Zeng, F. Zhao, R. Jiao, and C. Li, "On formulating and designing antenna arrays by evolutionary algorithms," *IEEE Trans. Antennas Propag.*, vol. 69, no. 2, pp. 1118–1129, Feb. 2021.

[5] A. Afsari, A. M. Abbosh, and Y. Rahmat-Samii, "Adaptive beamforming by compact arrays using evolutionary optimization of schelkunoff polynomials," *IEEE Trans. Antennas Propag.*, vol. 70, no. 6, pp. 4485–4497, Jun. 2022, doi: 10.1109/TAP.2022.3140347.

[6] Y.-X. Zhang, Y.-C. Jiao, and L. Zhang, "Antenna array directivity maximization with sidelobe level constraints using convex optimization," *IEEE Trans. Antennas Propag.*, vol. 69, no. 4, pp. 2041–2052, Apr. 2021.

[7] C. X. Yang, J. Zhang, and M. S. Tong, "A hybrid quantum-behaved particle swarm optimization algorithm for solving inverse scattering problems," *IEEE Trans. Antennas Propag.*, vol. 69, no. 9, pp. 5861–5869, Sep. 2021.

[8] C. Yang, J. Zhang, and M. S. Tong, "An FFT-accelerated particle swarm optimization method for solving far-field inverse scattering problems," *IEEE Trans. Antennas Propag.*, vol. 69, no. 2, pp. 1078–1093, Feb. 2021.

[9] J. Robinson and Y. Rahmat-Samii, "Particle swarm optimization in electromagnetics," *IEEE Trans. Antennas Propag.*, vol. 52, no. 2, pp. 397–407, Feb. 2004.

[10] Y. Rahmat-Samii and E. Michielssen, *Electromagnetic Optimization by Genetic Algorithms*. New York, NY, USA: Wiley, 1999.

[11] H. Liang, B. Wang, W. Liu, and H. Xu, "A novel transmitter placement scheme based on hierarchical simplex search for indoor wireless coverage optimization," *IEEE Trans. Antennas Propag.*, vol. 60, no. 8, pp. 3921–3932, Aug. 2012.

[12] J. Zhou, Z. Yang, Y. Si, L. Kang, H. Li, M. Wang, and Z. Zhang, "A trust-region parallel Bayesian optimization method for simulation-driven antenna design," *IEEE Trans. Antennas Propag.*, vol. 69, no. 7, pp. 3966–3981, Jul. 2021.

[13] S. Stadler and J. Igel, "Developing realistic FDTD GPR antenna surrogates by means of particle swarm optimization," *IEEE Trans. Antennas Propag.*, vol. 70, no. 6, pp. 4259–4272, Jun. 2022, doi: 10.1109/TAP.2022.3142335.

[14] M. Jing and G. Zhang, "Attributed scattering center extraction with genetic algorithm," *IEEE Trans. Antennas Propag.*, vol. 69, no. 5, pp. 2810–2819, May 2021.

[15] Z. Zhang, H. C. Chen, and Q. S. Cheng, "Surrogate-assisted quasi-Newton enhanced global optimization of antennas based on a heuristic hypersphere sampling," *IEEE Trans. Antennas Propag.*, vol. 69, no. 5, pp. 2993–2998, May 2021.

[16] G. Bogdan, K. Godziszewski, and Y. Yashchyshyn, "Time-modulated antenna array for real-time adaptation in wideband wireless systems—Part II: Adaptation study," *IEEE Trans. Antennas Propag.*, vol. 68, no. 10, pp. 6973–6981, Oct. 2020.

[17] E. Simsek, "Machine learning exercises on 1-D electromagnetic inversion," *IEEE Trans. Antennas Propag.*, vol. 69, no. 10, pp. 6797–6805, Oct. 2021.

[18] T. Brown and P. Mojabi, "Cascaded metasurface design using electromagnetic inversion with gradient-based optimization," *IEEE Trans. Antennas Propag.*, vol. 70, no. 3, pp. 2033–2045, Mar. 2022, doi: 10.1109/TAP.2021.3119115.

[19] A. Al-Saffar, A. Zamani, A. Stancombe, and A. Abbosh, "Operational learning-based boundary estimation in electromagnetic medical imaging," *IEEE Trans. Antennas Propag.*, vol. 70, no. 3, pp. 2234–2245, Mar. 2022, doi: 10.1109/TAP.2021.3111516.

[20] A. Afsari, "Mathematical models for efficient medical electromagnetic tomography," Ph.D. dissertation, ITEE School, Univ. Qld, St. Lucia, QLD, Australia, 2019.

[21] A. Afsari, A. M. Abbosh, and Y. Rahmat-Samii, "Modified born iterative method in medical electromagnetic tomography using magnetic field fluctuation contrast source operator," *IEEE Trans. Microw. Theory Techn.*, vol. 67, no. 1, pp. 454–463, Jan. 2019.

[22] M. Capek, L. Jelinek, and M. Gustafsson, "Shape synthesis based on topology sensitivity," *IEEE Trans. Antennas Propag.*, vol. 67, no. 6, pp. 3889–3901, Jun. 2019.

[23] M. N. Akinci, T. Çaglayan, S. Özgür, U. Alkasi, H. Ahmadzay, M. Abbak, M. Çayören, and I. Akduman, "Qualitative microwave imaging with scattering parameters measurements," *IEEE Trans. Microw. Theory Techn.*, vol. 63, no. 9, pp. 2730–2740, Sep. 2015.

[24] A. Pietrenko-Dabrowska and S. Koziel, "Expedited gradient-based design closure of antennas using variable-resolution simulations and sparse sensitivity updates," *IEEE Trans. Antennas Propag.*, vol. 70, no. 6, pp. 4925–4930, Jun. 2022, doi: 10.1109/TAP.2021.3138487.

[25] S. Koziel and A. Pietrenko-Dabrowska, "Accelerated gradient-based optimization of antenna structures using multifidelity simulations and convergence-based model management scheme," *IEEE Trans. Antennas Propag.*, vol. 69, no. 12, pp. 8778–8789, Dec. 2021.

[26] A. Afsari, A. M. Abbosh, and Y. Rahmat-Samii, "A rapid medical microwave tomography based on partial differential equations," *IEEE Trans. Antennas Propag.*, vol. 66, no. 10, pp. 5521–5535, Oct. 2018.

[27] S. K. Ghosh, S. Das, and S. Bhattacharyya, "Graphene-based metasurface for tunable absorption and transmission characteristics in the near mid-infrared region," *IEEE Trans. Antennas Propag.*, vol. 70, no. 6, pp. 4600–4612, Jun. 2022, doi: 10.1109/TAP.2022.3140904.

[28] V. Mishra and A. Kiourti, "Wearable electrically small loop antennas for monitoring joint flexion and rotation," *IEEE Trans. Antennas Propag.*, vol. 68, no. 1, pp. 134–141, Jan. 2020.

[29] R. Cicchetti, V. Cicchetti, A. Faraone, L. Foged, and O. Testa, "A compact high-gain wideband lens Vivaldi antenna for wireless communications and through-the-wall imaging," *IEEE Trans. Antennas Propag.*, vol. 69, no. 6, pp. 3177–3192, Jun. 2021.

[30] P. Tournier, M. Bonazzoli, V. Dolean, F. Rapetti, F. Hecht, F. Nataf, I. Aliferis, I. El Kanfoud, C. Migliaccio, M. de Buhan, M. Darbas, S. Semenov, and C. Pichot, "Numerical modeling and high-speed parallel computing: New perspectives on tomographic microwave imaging for brain stroke detection and monitoring," *IEEE Antennas Propag. Mag.*, vol. 59, no. 5, pp. 98–110, Oct. 2017.

[31] M. Hopfer, R. Planas, A. Hamidipour, T. Henriksson, and S. Semenov, "Electromagnetic tomography for detection, differentiation, and monitoring of brain stroke: A virtual data and human head phantom study," *IEEE Antennas Propag. Mag.*, vol. 59, no. 5, pp. 86–97, Oct. 2017.

[32] P. Mojabi, "Investigation and development of algorithms and techniques for microwave tomography," Ph.D. dissertation, Dept. Elect. Comp. Eng., Univ. Manitoba, Winnipeg, MB, Canada, 2010.

[33] D. Pliatsios, S. K. Goudos, T. Lagkas, V. Argyriou, A. A. Boulogeorgos, and P. Sarigiannidis, "Drone-base-station for next-generation Internet-of-Things: A comparison of swarm intelligence approaches," *IEEE Open J. Antennas Propag.*, vol. 3, pp. 32–47, 2022, doi: 10.1109/OJAP.2021.3133459.

[34] Z. Ž. Stankovic, D. I. Olcan, N. S. Doncov, and B. M. Kolundžija, "Consensus deep neural networks for antenna design and optimization," *IEEE Trans. Antennas Propag.*, vol. 70, no. 7, pp. 5015–5023, Jul. 2022, doi: 10.1109/TAP.2021.3138220.

[35] A. Afsari, P. De Souza, A. Abbosh, and Y. Rahmat-Samii, "Transistor laser antenna: Electromagnetic model in transmit and receive modes," *IEEE Access*, vol. 10, pp. 77498–77509, 2022.

[36] M. Rao and K. Sarabandi, "A low-profile dual-band dual-polarized quasi-endfire phased array for mmWave 5G smartphones," *IEEE Access*, vol. 10, pp. 38523–38533, 2022.

[37] J. C. Dash and D. Sarkar, "A four-port CSRR-loaded dual-band MIMO antenna with suppressed higher order modes," *IEEE Access*, vol. 10, pp. 30770–30778, 2022.

[38] J. C. Dash and D. Sarkar, "Microstrip patch antenna system with enhanced inter-port isolation for full-Duplex/MIMO applications," *IEEE Access*, vol. 9, pp. 156222–156228, 2021.

[39] Y. Huang and W. F. McColl, "An improved simplex method for function minimization," in *Proc. IEEE Int. Conf. Syst., Man Cybern. Inf. Intell. Syst.*, Beijing, China, Jan. 1996, pp. 1702–1705, doi: 10.1109/ICSMC.1996.565360.

**ARMAN AFSARI** (Member, IEEE) received the Ph.D. degree in electrical engineering from The University of Queensland, Brisbane, QLD, Australia, in 2019.

He is a Research Associate with the Electrical Engineering Department, University of Wisconsin–Madison. His research interests include computational electromagnetics, microwave imaging, radar beamforming, and matching networks.

Dr. Afsari was a recipient of the several IEEE conference awards, the Yazd University Special Talent Award, the University of Queensland Best Ph.D. Candidate Award, and the IEEE TRANSACTIONS ON ANTENNAS AND PROPAGATION Outstanding Reviewer Award. He is an Associate Editor of *Spacecraft and Satellites journal*.

**AMIN ABBOSH** (Fellow, IEEE) received the Ph.D. degree in engineering from The University of Queensland, St. Lucia, QLD, Australia, in 2013. He is a Professor and a Leader of the Electromagnetic Innovations (EMAGIN) Group and the former Head of the School of Information Technology and Electrical Engineering, The University of Queensland. He has authored or coauthored more than 400 articles on electromagnetic imaging systems, wideband passive microwave devices, and planar antennas. He was a recipient of the IEEE AP-S King Prize for the Best Paper published in the IEEE TRANSACTIONS ON ANTENNAS AND PROPAGATION (two times).

**YAHYA RAHMAT-SAMII** (Life Fellow, IEEE) received the Ph.D. degree in electrical engineering from the University of Illinois at Urbana–Champaign, Champaign, IL, USA, in 1975.

He is a Distinguished Professor, holder of the Northrop-Grumman Chair in electromagnetics, a member of the U.S. National Academy of Engineering (NAE), a Foreign Member of the Chinese Academy of Engineering (CAE) and the Royal Flemish Academy of Belgium for Science and the Arts, and the former Head of the Electrical Engineering Department, University of California at Los Angeles (UCLA), Los Angeles, CA, USA. He was a Senior Research Scientist with the Caltech/NASA's Jet Propulsion Laboratory. He has pioneering research contributions in diverse areas of electromagnetics, antennas, measurements and diagnostics techniques, numerical and asymptotic methods, satellite and personal communications, human/antenna interactions, RFID and implanted antennas in medical applications, frequency-selective surfaces, electromagnetic band-gap and metamaterial structures, applications of the genetic algorithms, and particle swarm optimizations. He has authored or coauthored more than 1100 technical journal and conference papers, written over 36 book chapters, and six books; and the holder of many patents. He has more than 20 cover-page IEEE publication articles.

Dr. Rahmat-Samii is a fellow of AMTA, ACES, EMA, and URSI. He was a recipient of the 2011 IEEE Electromagnetics Field Award. He was a recipient of the Henry Booker Award from URSI, in 1984, which is given triennially to the most outstanding young radio scientist in North America; the Best Application Paper Prize Award (Wheeler Award) of the IEEE TRANSACTIONS ON ANTENNAS AND PROPAGATION, in 1992 and 1995; the University of Illinois ECE Distinguished Alumni Award, in 1999; the IEEE Third Millennium Medal; and the AMTA Distinguished Achievement Award, in 2000. In 2001, he received the Honorary Doctorate Causa from the University of Santiago de Compostela, Spain. He also received the 2002 Technical Excellence Award from JPL, the 2005 URSI Booker Gold Medal at the URSI General Assembly, the 2007 IEEE Chen- To Tai Distinguished Educator Award, the 2009 Distinguished Achievement Award of the IEEE Antennas and Propagation Society, the 2010 UCLA School of Engineering Lockheed Martin Excellence in Teaching Award, and the 2011 Campus-Wide UCLA Distinguished Teaching Award. He was also a recipient of the Distinguished Engineering Educator Award from the Engineers Council, in 2015; the John Kraus Antenna Award of the IEEE Antennas and Propagation Society; the NASA Group Achievement Award, in 2016; the ACES Computational Electromagnetics Award; the IEEE Antennas and Propagation Society S. A. Schelkunoff Best Transactions Prize Paper Award, in 2017; and the Harrington–Mittra Award in Computational Electromagnetics, in 2022. He was also a recipient of the prestigious Ellis Island Medal of Honor, in 2019. The medals are awarded annually to an exceptionally small group of distinguished U.S. citizens who exemplify a life dedicated to community service. These are individuals who preserve and celebrate the history, traditions, and values of their ancestry while exemplifying the values of the American way of life and are dedicated to creating a better world. Among the recipients of this honor are seven former presidents of the United States of America, to name a few. He is listed in Who's Who in America, Who's Who in Frontiers of Science and Technology, and Who's Who in Engineering. He has been a plenary and millennium session speaker at numerous national and international symposia. He was an organizer and a presenter of many successful short courses worldwide. Many of his students have won major theses and conference paper awards and hold senior positions in academia and industry. He is the Designer of the IEEE Antennas and Propagation Society Logo, displayed on all the official correspondence of the IEEE Antennas and Propagation Society. He was the President of the IEEE Antennas and Propagation Society, in 1995, and the United States National Committee (USNC) of the International Union of Radio Science (URSI), from 2009 to 2011. He has served as an IEEE Distinguished Lecturer, presented lectures internationally.

● ● ●